Enhanced O_2 selectivity of carbon molecular sieves by electrochemical oxidation for air separation

Urita, Koki
Graduate School of Integrated Science and Technology, Nagasaki University

Ishida, Takashi
Graduate School of Integrated Science and Technology, Nagasaki University

Marubayashi, Kaito
Graduate School of Engineering, Nagasaki University

Tanaka, Hideki
Institute for Aqua Regeneration (ARG), Shinshu University

他

出版情報：Carbon. 235, pp.120088-, 2025-03-10. Elsevier
バージョン：

Carbon 235 (2025) 120088

Contents lists available at ScienceDirect

Carbon

journal homepage: www.elsevier.com/locate/carbon

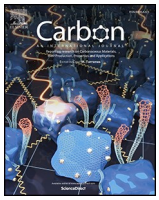

Enhanced O_2 selectivity of carbon molecular sieves by electrochemical oxidation for air separation

Koki Urita [a,*], Takashi Ishida [a,b], Kaito Marubayashi [c], Hideki Tanaka [d], Miyu Hamasaki [c], Yasuyuki Yamane [b], Jin Miyawaki [e], Hiroo Notohara [a], Isamu Moriguchi [a]

[a] Graduate School of Integrated Science and Technology, Nagasaki University, 1-14 Bunkyo-machi, Nagasaki, 852-8521, Japan
[b] Research & Development Dept., Activated Carbon Business Div., Osaka Gas Chemicals Co., Ltd., 5-11-61, Torishima, Konohana-ku, Osaka, 554-0051, Japan
[c] Graduate School of Engineering, Nagasaki University, 1-14 Bunkyo-machi, Nagasaki, 852-8521, Japan
[d] Institute for Aqua Regeneration (ARG), Shinshu University, 4-17-1 Wakasato, Nagano, 380-8553, Japan
[e] Institute for Materials Chemistry and Engineering, Kyushu University, 6-1 Kasugakoen, Kasuga, Fukuoka, 816-8580, Japan

ARTICLE INFO

Keywords:
Carbon molecular sieves
Air separation
Electrochemical oxidation
Adsorption rate

ABSTRACT

We propose a novel method for synthesizing carbon molecular sieves (CMS) with enhanced performance for O_2 separation from air using flow-type electrochemical oxidation (F-ECO). The F-ECO process introduces oxygen-containing functional groups (OCFGs) at pore entrances of activated carbon (AC), creating an ultrathin layer that works as an energy barrier for improving O_2 selectivity. The parameters for the F-ECO process were optimized using an experimental design method. The microstructure and surface species of the F-ECO-treated AC samples were characterized using X-ray photoelectron spectroscopy and gas adsorption measurements. The F-ECO treatment slightly reduced micropore volume but dramatically increased the O_2 dynamic selection coefficient of AC, indicating improved N_2/O_2 separation. The optimal F-ECO conditions produced a CMS with O_2 selectivity comparable to the CMS provided by conventional methods in industry, along with a faster O_2 adsorption rate while minimizing the decrease in effective O_2 adsorbed amount. This performance was achieved by carefully controlling the surface oxidation proposed by the experimental design method based on Bayesian optimization. The results demonstrate the potential of this approach for developing energy-efficient O_2 enrichment technologies.

1. Introduction

Reducing energy consumption is required to achieve a sustainable society on a global scale. Most combustion systems are operated under a 21 % oxygen concentration restriction in the combustion air, regardless of the fuel type. Fuel consumption can be reduced by approximately 30 % under oxygen-enriched air, increasing the oxygen concentration from 21 % to 30 % [1]. Oxygen-enriched air also effectively improves the CO_2 concentration in flue gas [2,3]. Larbi et al. indicated that increasing the CO_2 concentration reduces the regeneration energy and carbon recycling cost of flue gas. Fuels like carbon-neutral and biomass fuels often have low calorific values and variable properties, which can lead to unstable combustion [4]. Using oxygen-enriched air can help achieve stable combustion, even such fuels, and improve the efficiency of combustion equipment. Cryogenic air separation methods [5,6] and pressure swing adsorption (PSA) methods [7–11] have been widely used to produce large volumes of oxygen-enriched air. The cryogenic separation method consumes much energy to separate N_2 and O_2, requiring a high air pressure of about 0.5 MPa and a low air temperature of around −200 °C. The PSA method produces highly concentrated oxygen (90–95 %). However, the power consumption is large owing to the pressure loss at the adsorbent packing column and decompression regeneration. The energy-saving effects of the current processes are still low, and the combustion costs remain high to concentrate oxygen up to a few 10 % from the air. Thus, oxygen enrichment results in extra power consumption in the oxygen concentration process, making it difficult to save energy for the entire combustion system.

The thermal swing adsorption (TSA) method is expected to save energy by utilizing the heat exhausted during combustion [12,13]. Oxygen collected from air into the adsorbents below approximately 40 °C is released as oxygen-enriched air during the heating regeneration process. Zeolites with controlled pore sizes have been widely used as adsorbents

* Corresponding author.
E-mail address: urita@nagasaki-u.ac.jp (K. Urita).

https://doi.org/10.1016/j.carbon.2025.120088
Received 3 November 2024; Received in revised form 9 January 2025; Accepted 4 February 2025
Available online 5 February 2025

for gas separation at the TSA process [14,15]. Eriksson et al. reported that the TSA process produces oxygen-enriched air at the concentration of 30 % using zeolite as an adsorbent [16]. However, water in the air must be removed before the air passes through the zeolite adsorbent due to preferential water adsorption. Porous carbons have the potential to be used as oxygen adsorbents, unaffected by water, because they form lower hydrophilic surfaces than zeolites [17]. The micropores in porous carbons do not form ordered networks adjusting to O_2 size, being different from zeolites where the gas separation can be achieved by the pore size control. Carbon molecular sieves (CMS) have been widely used as an adsorbent for the gas separation process [18–21]. The CMS kinetically recovers a target molecule from mixture gases by controlling the pore entrance size of porous carbons even if the molecular size difference is less than 1 Å [22,23]. A typical technique for functionalizing the molecular sieving ability to porous carbons is chemical vapor deposition (CVD), in which amorphous carbon is deposited at the pore entrance to narrow the diameter of the entrance [24]. Yamane et al. indicated that the deposited carbon acts as an energy barrier for gas molecules to enter the pores and that this energy barrier enables CMS to kinetically separate molecules [23,25]. They also suggested that the thicker the carbon membrane, the lower the adsorption rate into the pore; narrowing the pore entrance with a thin membrane can increase the efficiency of the recovery of target molecules. Regarding molecular transport, Vallejos-Burgos et al. theoretically suggested that oxygen-containing functional groups (OCFGs) at nanowindows in a graphene sheet contribute to air separation [26]. The transport of N_2 and O_2 molecules through the nanowindows is strongly influenced by the partial charge distribution derived from OCFGs and the dynamic motion of the OCFGs.

In this study, we propose a new method for CMS synthesis by applying electrochemical oxidation (ECO) to a microporous carbon in aqueous electrolytes. Since the ECO process against carbon creates OCFGs at unstable sites such as graphite edges and defective parts in the surface [27,28], the OCFGs added at the pore entrance are expected to work as an ultrathin barrier layer for N_2/O_2 separation. This method for surface oxidation of carbons does not require strong oxidants leading to corrosion of the ECO-cell and thermal treatment leading to a large structural change of carbon frameworks. Additionally, the oxidation degree is easily controlled by conditions such as applied voltage, pH of electrolytes, and oxidation time [29]. Yue et al. reported that phenolic, lactone, and carboxyl groups are formed on the surface of activated carbons at an applied voltage of 0.5 V, 0.5–1.5 V, and 1.5 V or higher, respectively [30]. In the case of highly oriented pyrolytic graphite (HOPG), the edges of HOPG were terminated by phenolic and carbonyl groups between 0.2 and 1.0 V, and the surface oxidation was accelerated at 1.0 V [31,32]. Previous ECO processes were performed in batch mode using carbon electrodes mixed with a binder in a circulating acid or alkali solution. However, the batch mode requires a molding process for the powdered porous carbon, fixation to the electrodes, and replacement of the electrodes after the surface oxidation, whose processes increase its environmental impact and make it unsuitable for industrialization. Volker et al. showed a new concept called an electrochemical flow capacitor in which an electric-double layer is formed on porous carbons in an electrolyte suspension [33]. This flow-type electrochemical reaction system was not limited to energy storage devices but was also applied to seawater desalination [34]. The flow system is expected that OCFGs are added to porous carbon powder suspended in an electrolyte solution. We applied a flow-type ECO (F-ECO) to synthesize a CMS with an extremely thin gate at the pore entrance for N_2 and O_2 separation. The F-ECO conditions, such as voltage, time, temperature, and pH of the acid solution, were optimized by introducing an experimental design method. The porous carbons with OCFGs provided by F-ECO showed high N_2/O_2 separation performance; the O_2 adsorption rate of the obtained CMS was 10 times faster than that of conventional CMS. Our results indicate that OCFGs work as an extremely thin gate at the pore entrance for N_2/O_2 separation.

2. Experimental

2.1. Synthesis of surface oxidized porous carbons by F-ECO

Activated carbon (AC) derived from coconut shells was used as the base carbon for CMS. Since the maximum O_2 effective adsorbed amount ($EAA[O_2]$) is expected to be obtained on AC with an average pore size of 0.44 nm from theoretical analysis of O_2 adsorption isotherms at 25 °C and 80 °C under 20 kPa, we prepared the AC with a central pore size of around 0.44 nm in the pore size distribution (PSD). $EAA[O_2]$ is the amount of O_2 that can be recovered by desorption at 80 °C from the O_2 adsorbed at 25 °C and 20 kPa. This value was determined by subtracting the adsorbed amount at 80 °C from that at 25 °C. The AC powder with a particle size of approximately 150 μm was collected using a 100-mesh sieve for the F-ECO. AC (200 mg) was added to 200 mL of a sulfuric acid solution at a given concentration to prepare a suspension of AC. The experimental setup for the F-ECO treatment consisted of a reservoir, a liquid pump without pulsation (FW2-LD-240, Surpass Industry Co., Ltd.), and a voltage-applying cell (C-Flow 5 × 5 Electrochemical Research Cell, C-Tech Innovation), each of which was connected to a tube with a diameter of 4 mm (Fig. 1). The pumping speed was set at 27.5 ml/min. The voltage-applying cell was heated between 25 and 80 °C using a jacket heater manufactured by Kawai Corporation. Voltage was applied between 0 and 1.5 V using a DC-stabilized power supply (PMX18-2A, Kikusui Electronics Corp.). The experimental condition was optimized by using an experimental design method [35]. The F-ECO treated AC samples are named as CMS-E*X* (*X*: sample number).

2.2. Experimental designs for F-ECO

Table 1 shows the experimental conditions for CMS-E*X* production in F-ECO estimated from the parameters. The total number of experiments reached $7 \times 16 \times 12 \times 12 = 16{,}128$. We applied Bayesian optimization based on Gaussian process regression to the experimental design to efficiently optimize the experimental parameters under a vast number of experimental conditions (see in Supporting Information I). The D-optimal designs were applied to select 10 experimental candidates characterized by minimal correlation coefficients among their respective experimental parameters, drawn from 16,128 potential experimental conditions. The CMS-E*X* samples were prepared based on 10 experimental candidates. The adsorption time constant ($t_{0.5}$), the dynamic selection coefficient of O_2 ($DSC[O_2]$), and the $EAA[O_2]$ were experimentally evaluated. The adsorption time constants are the time at which the adsorption fraction becomes 0.5 at the equilibrium adsorption pressure of 20 kPa for O_2 and 80 kPa for N_2. The parameter helps to assess the kinetic adsorption of O_2 over N_2 [25]. The $DSC[O_2]$ is the rate of adsorption time constant ($t_{0.5}[N_2/O_2]$) of N_2 ($t_{0.5}[N_2]$) against that of O_2 ($t_{0.5}[O_2]$): the faster the adsorption rate of O_2 and the slower the adsorption rate of N_2, the larger the $DSC[O_2]$. Based on the experimental results, a numerical model was constructed using the Gaussian process regression method based on the $DSC[O_2]$ and $t_{0.5}$ as objective variables. Bayesian optimization method was applied by using this model to derive candidate experimental conditions to maximize the $DSC[O_2]$ and minimize $t_{0.5}$. Additionally, CMS-E*X* (X = 11–13) was provided under different conditions at pH = 1 to evaluate the validity of the final solution. Table 2 shows the 10 candidate experiments (X = 1–10) derived from the design of experiments, comparison experiments at pH = 1 (X = 11–13), the second candidate (X = 14), and the final solutions derived from them (X = 15).

2.3. Characterization

The microstructure of the AC was directly observed by high-resolution scanning transmission electron microscopy (ARM200CF, JEOL Ltd.) in transmission mode (HR-TEM). An acceleration voltage was set at 120 kV to prevent the morphological changes by electron

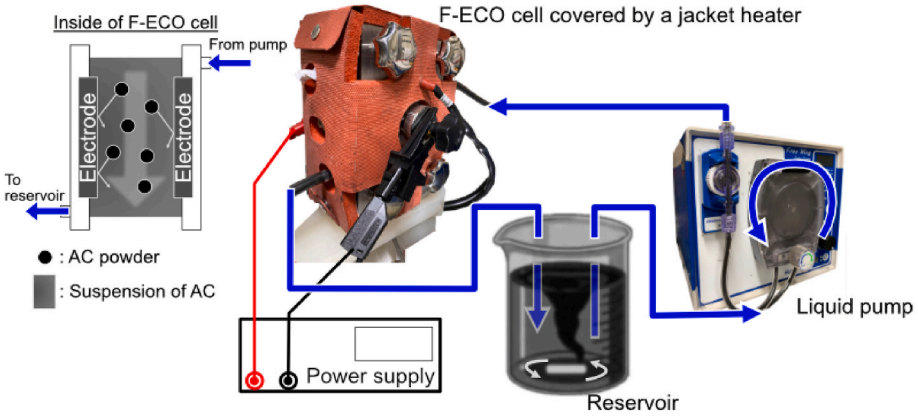

Fig. 1. Schematic of the experimental setup for the F-ECO.

Table 1
Experimental parameters for CMS synthesis by the F-ECO method.

Condition	Range	Step	Number of parameters
pH	1.0–7.0	1.0	7
Applied voltage [V]	0–1.5	0.1	16
Applied time [h]	0.5–6.0	0.5	12
Temperature [°C]	25–80	5.0	12

Table 2
1st ($X = 1$–10) and 2nd ($X = 14$) candidates, comparison ($X = 11$–13) and final ($X = 15$) experimental conditions for CMS synthesis.

Sample number, X	pH	Applied voltage [V]	Applied time [h]	Temperature [°C]
1	1	0.5	2.5	55
2	2	1	1.5	70
3	3	1.3	0.5	25
4	4	0.3	1.5	25
5	7	1.1	5.5	25
6	5	0.1	0.5	60
7	1	0.6	5.5	65
8	6	0.3	2	50
9	6	0.9	3.5	80
10	4	N/A	6	45
11	1	1	1.5	25
12	1	1	3	25
13	1	1	6	25
14	**1**	**1.5**	**6**	**35**
15	**1**	**1.5**	**4.5**	**35**

irradiation [36,37]. X-ray photoelectron spectroscopy (XPS) was performed to clarify the degree of oxidation of the surface of the AC samples before and after the F-ECO treatment. The C1s and O1s spectra were collected using a KRATOS ULTRA (Shimadzu Co., Ltd.) with monochromatic Al Kα radiation. The bonding information in the C1s and O1s spectra of a carbon sticker used to fix the samples was removed by covering the entire surface of the carbon sticker with pelletized samples. The oxygen/carbon (O/C) ratio was determined from deconvoluted curves in the O1s and C1s peaks fitted by the Voigt function [38].

Since the pore size of our target carbons is below 1.2 nm, the CO_2 adsorption isotherm at 25 °C is applied to evaluate the porous structure. N_2 adsorption isotherms at 77 K and Ar adsorption isotherms at 87 K have been widely applied to evaluate the porous structure of porous carbons. However, the diffusion and penetration of adsorbate molecules in pores are very slow at such low temperatures. Accurate analysis of micropores cannot be achieved under these conditions because of insufficient measurement points at low relative pressure, including information on micropores. In contrast, the CO_2 adsorption isotherm up to atmospheric pressure at 25 °C does not allow the evaluation of mesopores but includes structural information on micropores below a pore size of 1.2 nm. Since the pore entrances and internal pores of CMS are extremely narrow, it is expected that probe gas molecules will struggle to pass through these pore entrances and reach the deep interior of the pores at low temperatures. Therefore, CO_2 adsorption isotherms of CMS and their precursor-AC were measured at 25 °C. The PSDs were determined by fitting kernels obtained from the grand canonical Monte Carlo (GCMC) method applying to carbon slit pores to the experimental isotherms at 25 °C. The detailed procedure to determine the kernels is shown in Supporting Information II. The CO_2 adsorption isotherms were measured after pre-evacuation at 80 °C for 6 h (BELSORP-max and BELSORP-maxII, MicrotracBEL Corp.). The pre-evacuation condition was set to remove only adsorbates while preventing the removal of functional groups on the carbon surfaces. The EAA[O_2] was determined by subtracting the adsorbed amount of O_2 at 20 kPa at 25 °C and 80 °C. Raising the O_2 desorption temperature improves regeneration efficiency. However, if the carboxyl group mainly acts as the separation gate, decomposition begins at around 100 °C [28]. We assumed the recovery of O_2 from waste heat at 80 °C, and the EAA[O_2] was evaluated as the desorption temperature of 80 °C. The adsorption rates of O_2 and N_2 were measured at 20 kPa and 80 kPa, respectively, corresponding to the partial pressure in the atmosphere. The kinetic separation performances were assessed from the value of DSC[O_2] and EAA[O_2], as well as the ratio of the diffusion coefficient determined from the multiple linear driving force (LDF) equation and the rate constant [25,39].

3. Result and discussion

The HR-TEM images clearly show the carbon frameworks of the AC before the F-ECO treatment (Fig. 2a and b). The AC consists of micrographites (Fig. 2a), with pore entrances facing each other of the carbon surfaces with large curvature and the micrographite edges (Fig. 2b). Since the structural stability of carbon frameworks tends to decrease with increasing curvature [40,41], carbon surfaces with high curvature are more reactive than flat surfaces, similar to the edge and defective sites. The OCFGs should likely be introduced at the pore entrance during AC fabrication and oxidation processes. The PSDs of representative samples show the porosity change of AC by the F-ECO treatment (Fig. 2c). Since the PSD reflects the rate of internal pore spaces rather than the pore entrance size, the reduction in the PSD suggests the internal space of the pore was narrowed by the addition of OCFGs on pore walls. The F-ECO treatment reduced pores above 0.42 nm. The sulfuric acid solution might have penetrated inside of such large pores, and the pore walls were also oxidized. Although the CMS-E15 obtained by optimum treatment conditions showed a reduction of pores with a pore size until 0.55 nm, the pores at higher pore sizes were retained to the same degree as the AC sample. Maintaining pores that allow O_2 to pass

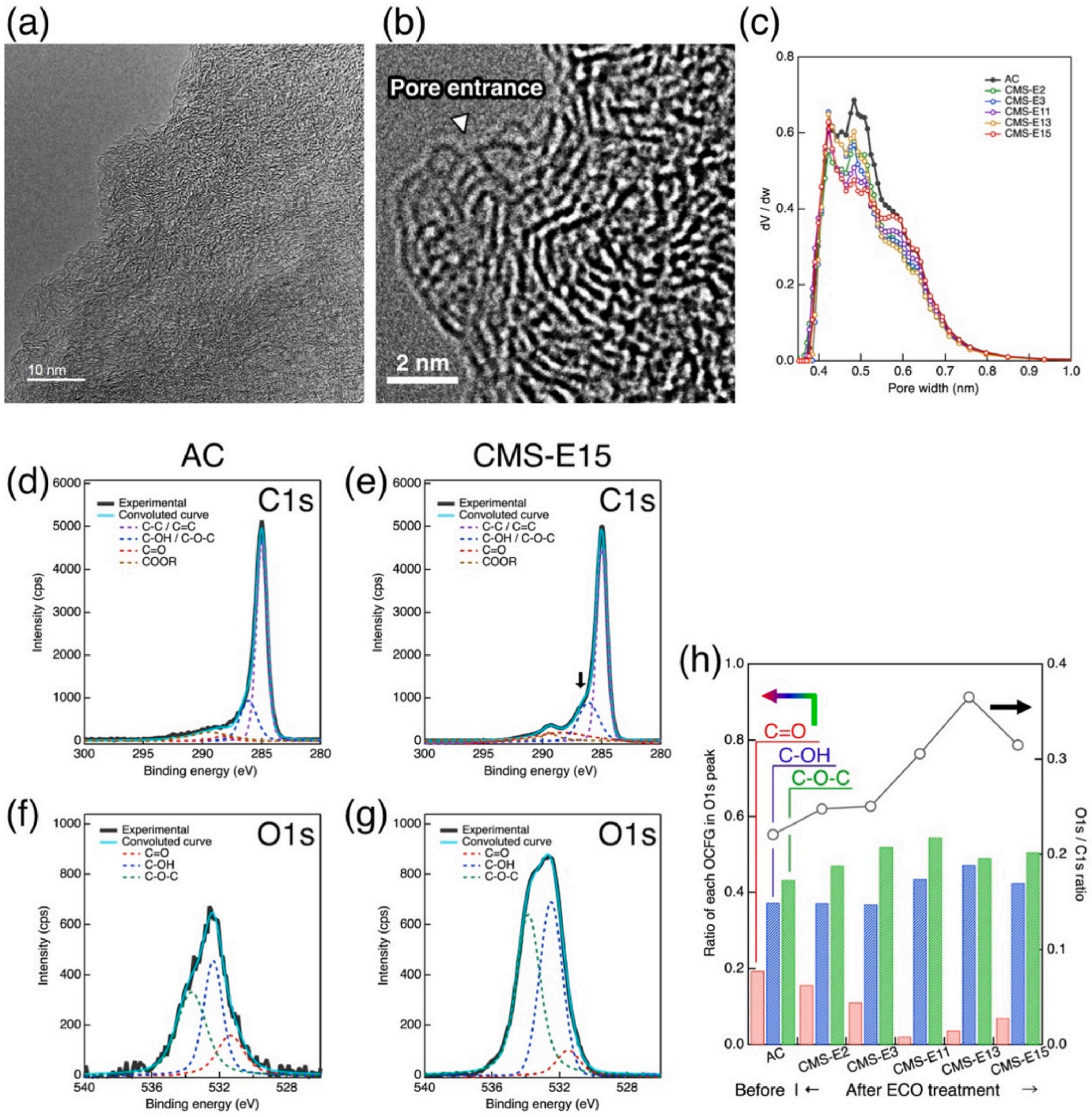

Fig. 2. HR-TEM images of the entire (a) and surface (b) of AC without F-ECO treatment. (c) PSD of representative samples determined from CO_2 adsorption isotherms at 25 °C. XPS spectra of AC (d, f) and CMS-E15 (e, g). (d) and (e) are C1s spectra and (f) and (g) are O1s spectra. Black arrow in (e) points out shoulder peak derived from hydroxyl and epoxide. (h) Ratio of OCFGs (red: carbonyl, blue: hydroxyl, and green: epoxide) and O/C ratio (black open circle) of AC and representative CMS-E*X* (*X* = 2, 3, 11, 13 and 15). (For interpretation of the references to colour in this figure legend, the reader is referred to the Web version of this article.)

should prevent the decrease in EAA[O_2]. The degree of addition of OCFGs to AC by the F-ECO was evaluated using the C1s (Fig. 2d and e) and O1s (Fig. 2 f and g) XPS spectra with deconvoluted results. The most substantial peak at 285.6 eV was assigned to the carbon-carbon bond, which is a combination of sp^2 and sp^3 bonds. Other subpeaks were assigned to the OCFGs of hydroxyl (C–OH) and epoxide (C–O–C) at 286.8 eV, carbonyl (C═O) at 289.1 eV, and carboxylic (COO) at 290 eV [42]. The C1s spectrum of CMS-E15 (Fig. 2e) exhibited a shoulder peak of around 286.8 eV compared to AC (Fig. 2d), mainly derived from hydroxyl groups and epoxide. Since the hydroxyl groups and epoxide are the predominant OCFGs in the CMS-E*X* samples, the decomposition of OCFGs is not expected to occur until 500 °C [28]; separation gates by OCFGs are stable in the regeneration process. The increase in OCFGs in CMS-E15 was clearly represented in the O1s XPS spectrum. The deconvoluted curves were assigned to carbonyl (C═O) at 531.4 eV, hydroxyl (C–OH) at 532.5 eV, and epoxide (C–O–C) at 533.8 eV. Fig. 2h shows the presence ratios of each OCFG obtained from the areas of the deconvoluted curves against overall O1s spectra and the area ratio of the

O1s spectrum against the C1s spectrum (O/C ratio) on randomly selected samples. The O/C ratio of CMS-E*X* samples was increased compared with that of AC; the OCFGs were introduced to the AC passing through the F-ECO process. F-ECO treatment at applied voltages above 1 V decreased carbonyl bonding and increased the hydroxyl group and the epoxide. CMS-E15 exhibited a lower O/C ratio than CMS-E13, in which the pores were reduced between the pore size of 0.50 nm and 0.55 nm, suggesting that adding excess OCFGs in micropores of CMS-E13 might cause performance degradation in CMS.

The adsorbability of oxygen on AC and CMS-E*X* samples was estimated by the differential of the adsorbed amount of O_2 at 20 kPa at 25 °C and 80 °C. Fig. 3a shows O_2 adsorption isotherm at 25 °C and 80 °C of AC, and CMS-E15. The EAA[O_2] of samples was calculated from the adsorbed amount at 20 kPa in each adsorption isotherm (Fig. 3b). The EAA[O_2] of CMS-E*X* samples was lower than that of AC. The decrease in EAA[O_2] is linked to a reduction in micropore volume, as represented by the PSD (Fig. 2c); the addition of OCFGs also occurred in the micropores by the F-ECO. Previous reports suggested that the ECO treatment under high applied voltage and low pH accelerates the addition of OCFGs and increases the surface oxygen content [30,43]. Compared to previous reports, the relatively mild oxidation conditions for CMS-E6 may prevent the decrease in EAA[O_2]. In contrast, CMS-E10, produced under mild oxidation conditions without voltage application, represented a significant decrease in the EAA[O_2]. This opposing trend suggests that numerous systematic tests are necessary to determine optimal conditions based on the relationship between EAA[O_2] and each F-ECO condition. Fig. 3c shows the relationship between the EAA[O_2] and the O/C ratio. The EAA[O_2] decreased as the O/C ratio increased. When comparing CMS-E15 with CMS-E11, which represents similar O/C ratios, the EAA[O_2] of CMS-E15 was higher even with increasing O/C ratios. Accordingly, the experimental design method is effective for efficiently finding the optimal condition among multiple experimental parameters.

The DSC[O_2] was determined from the adsorption rate curves of O_2 and N_2 for each sample. The adsorption rate curves (Fig. 4a and b and Supporting Information Fig. S4) are obtained from the adsorption fraction, which is the adsorbed amount at each time relative to the equilibrium adsorbed amount. The adsorption rate curves for O_2 and N_2 overlapped in AC (Fig. 4a), indicating that separating these gases is not feasible. In contrast, in CMS-E*X* (Fig. 4b and Supporting Information Fig. S4), the O_2 adsorption rate curves represented faster than those for N_2. The addition of OCFGs should maintain the O_2 adsorption rate while only slowing the N_2 adsorption rate. Fig. 4c shows the performance of EAA[O_2] and DSC[O_2] of each sample. As mentioned before, the EAA[O_2] was decreased with the F-ECO treatment due to the introduction of OCFGs in the micropores. Conversely, the DSC[O_2] substantially increased with the F-ECO treatment. The separation performance for O_2 and N_2 was markedly improved due to the increase in OCFGs at the pore entrance. The improvement of separation performance seems primarily to depend on the amount of OCFG, which creates narrow pore entrances, rather than the type of OCFG (Supporting Information, Fig. S5). However, the increase in OCFGs by adding hydroxyl groups and epoxides led to the enhancement of DSC[O_2]. This suggests that modifying the proportions of OCFG types is essential for enhancing N_2/O_2 separation performance. The rate constants (k_{LDF}) for O_2 and N_2 were determined from the distribution of k_{LDF} (Supporting Information, Fig. S6)

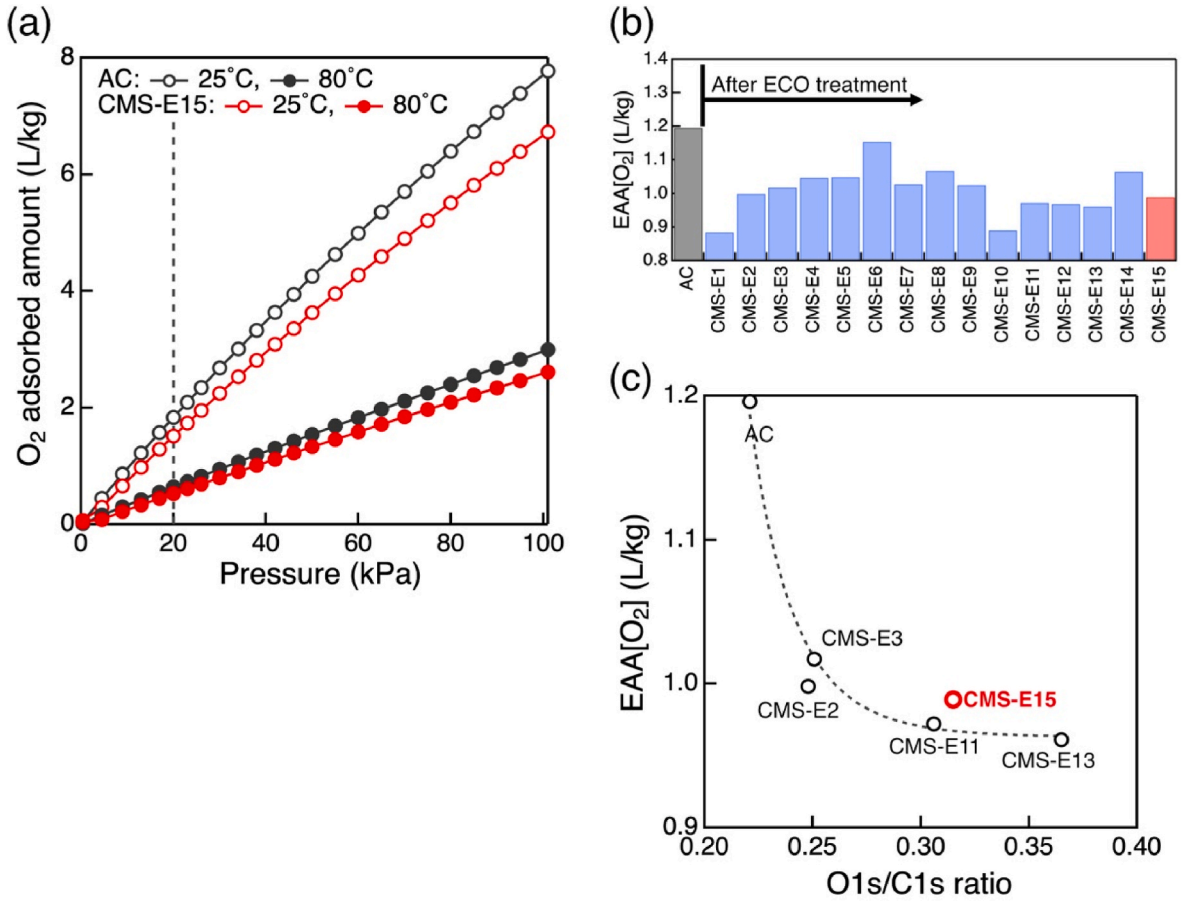

Fig. 3. (a) O_2 adsorption isotherms at 25 °C and 80 °C for AC and CMS-E15. The broken line shows oxygen partial pressure. (b) EAA[O_2] for each sample obtained from subtracting the adsorbed amount at 80 °C from the adsorbed amount at 25 °C at 20 kPa of oxygen partial pressure. (c) Relationship between EAA[O_2] and O1s/C1s ratio calculated from XPS in Fig. 2(h).

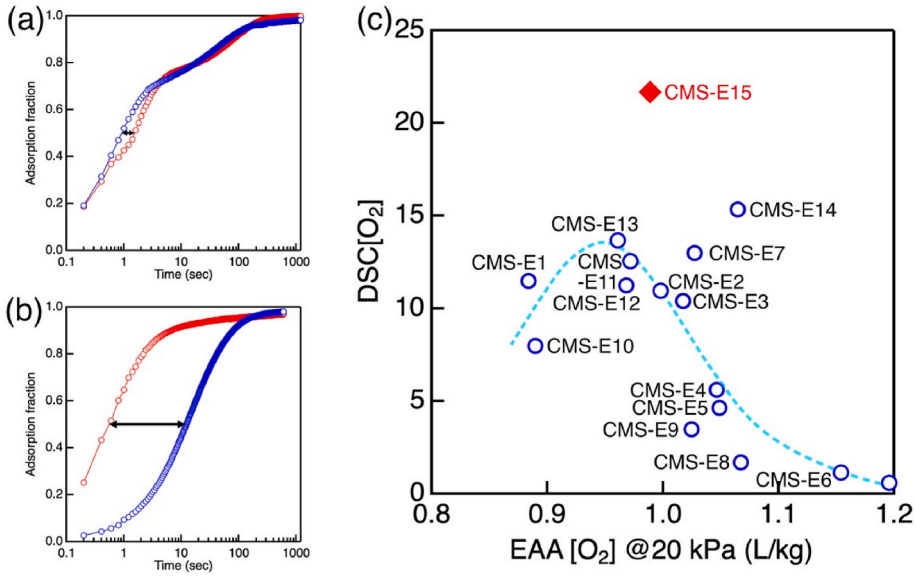

Fig. 4. Adsorption rate curves of O_2 (red open circle) and N_2 (blue open circle) for AC (a) and CMS-E15 (b). The black double-ended arrows represent the difference in adsorption rate at the adsorption fraction of 0.5. Adsorption rate curves of other CMS-E*X* samples are shown in Supporting Information (Fig. S4). (c) CMS performance on DSC[O_2] and EAA[O_2] for AC and CMS-E*X* samples. The F-ECO conditions of CMS-E15 were determined by the experimental design method. (For interpretation of the references to colour in this figure legend, the reader is referred to the Web version of this article.)

calculated from a multiple LDF equation to compare the separation performance with previous works. The detailed procedure to estimate the distribution of k_{LDF} has been reported by Yamane et al. [25]. The comparison of the rate constant of O_2 (k_{O2}) and the O_2/N_2 kinetic selectivity for results obtained in this work and previous works indicated that CMS-E15 has the highest k_{O2} and approaches the O_2/N_2 kinetic selectivity exhibited by CMS produced through the CVD process (Supporting Information, Fig. S7). This indicates that the new process to provide CMS has potential for practical applications in gas separation processes.

4. Conclusion

Using the F-ECO method, we have proposed a new synthesis route for CMS with enhanced O_2 and N_2 separation performance. By optimizing the parameters of the F-ECO condition obtained from the experimental design method, we significantly improved O_2 selectivity while minimizing the reduction in EAA[O_2]. A key innovation in our approach was the incorporation of OCFGs at the entrances of the pores at AC to provide the CMS for O_2 and N_2 separation. The modification against the pore entrance, creating an ultrathin barrier layer, dramatically increased the oxygen adsorption rate constant compared to the CMS provided by the CVD method. These results indicate the potential of the F-ECO technique as a highly effective and environmentally sustainable method for generating high-performance CMS tailored for oxygen enrichment applications. Further exploration of the optimization for process parameters and the methodologies for scaling up the F-ECO process could significantly contribute to developing more energy-efficient and cost-effective technologies for oxygen enrichment across diverse industrial settings.

CRediT authorship contribution statement

Koki Urita: Writing – original draft, Visualization, Supervision, Resources, Project administration, Methodology, Investigation, Conceptualization. **Takashi Ishida:** Writing – review & editing, Investigation. **Kaito Marubayashi:** Investigation. **Hideki Tanaka:** Writing – original draft, Resources, Methodology, Investigation, Formal analysis. **Miyu Hamasaki:** Investigation. **Yasuyuki Yamane:** Writing – review & editing, Resources. **Jin Miyawaki:** Writing – review & editing. **Hiroo Notohara:** Writing – review & editing, Investigation. **Isamu Moriguchi:** Writing – review & editing, Resources.

Declaration of competing interest

The authors declare that they have no known competing financial interests or personal relationships that could have appeared to influence the work reported in this paper.

Acknowledgment

This study was supported by the New Energy and Industrial Technology Development Organization (NEDO).

Appendix A. Supplementary data

Supplementary data to this article can be found online at https://doi.org/10.1016/j.carbon.2025.120088.

References

[1] Y. Chang, K. Wu, Y. Chen, C. Chen, Atomized air of oxygen-enriched combustion for a 450 000 kcal/h industrial furnace, Energy Fuel. 29 (5) (2015) 3476–3482.
[2] S. Laribi, L. Dubois, G. De Weireld, D. Thomas, Study of the post-combustion CO_2 capture process by absorption-regeneration using amine solvents applied to cement plant flue gases with high CO_2 contents, Int. J. Greenh. Gas Control 90 (2019) 102799.
[3] C. Feng, R. Zhu, G. Wei, K. Dong, J. Dong, Typical case of carbon capture and utilization in Chinese iron and steel enterprises: CO_2 emission analysis, J. Clean. Prod. 363 (2022) 132528.
[4] S. Baetge, M. Kaltschmitt, Rice straw and rice husks as energy sources-comparison of direct combustion and biogas production, Biomass Convers. Biorefin. 8 (3) (2018) 719–737.
[5] A.R. Smith, J. Klosek, A review of air separation technologies and their integration with energy conversion processes, Fuel Process. Technol. 70 (2) (2001) 115–134.
[6] K. Zhang, J. Sunarso, Z. Shao, W. Zhou, C. Sun, S. Wang, S. Liu, Research progress and materials selection guidelines on mixed conducting perovskite-type ceramic membranes for oxygen production, RSC Adv. 1 (9) (2011) 1661–1676.
[7] S. Farooq, D.M. Ruthven, H.A. Boniface, Numerical simulation of a pressure swing adsorption oxygen unit, Chem. Eng. Sci. 44 (12) (1989) 2809–2816.
[8] S. Sircar, B.F. Hanley, Production of oxygen enriched air by rapid pressure swing adsorption, Adsorption 1 (4) (1995) 313–320.
[9] S. Hayashi, M. Kawai, T. Kaneko, Dynamics of high purity oxygen PSA, Gas Sep. Purif. 10 (1) (1996) 19–23.

[10] R.V. Siriwardane, M.-S. Shen, E.P. Fisher, Adsorption of CO_2, N_2, and O_2 on natural zeolites, Energy Fuel. 17 (3) (2003) 571–576.
[11] J.C. Santos, F.D. Magalhães, A. Mendes, Contamination of zeolites used in oxygen production by PSA: effects of water and carbon dioxide, Ind. Eng. Chem. Res. 47 (16) (2008), 6197ç6203.
[12] J.A. Mason, K. Sumida, Z.R. Herm, R. Krishna, J.R. Long, Evaluating metal-organic frameworks for post-combustion carbon dioxide capture via temperature swing adsorption, Energy Environ. Sci. 4 (8) (2011) 3030–3040.
[13] R. Ben-Mansour, M.A. Habib, O.E. Bamidele, M. Basha, N.A.A. Qasem, A. Peedikakkal, T. Laoui, M. Ali, Carbon capture by physical adsorption: materials, experimental investigations and numerical modeling and simulations – a review, Appl. Energy 161 (2016) 225–255.
[14] A.A. Tishin, Study of adsorption properties of zeolites NaX, CaA, and CaNaA in separation of air components, Petrol. Chem. 60 (8) (2020) 964–970.
[15] E. Pérez-Botella, S. Valencia, F. Rey, Zeolites in adsorption processes: state of the art and future prospects, Chem. Rev. 122 (24) (2022) 17647–17695.
[16] T. Eriksson, Y. Kiros, Temperature swing adsorption device for oxygen-enriched air, J. Clean. Prod. 76 (2014) 174–179.
[17] N.F. Gao, S. Kume, K. Watari, Zeolite–carbon composites prepared from industrial wastes: (I) Effects of processing parameters, Mater. Sci. Eng., A 399 (1) (2005) 216–221.
[18] S.P. Nandi, P.L. Walker, Carbon molecular sieves for the concentration of oxygen from air, Fuel 54 (3) (1975) 169–178.
[19] H.J. Schröter, Carbon molecular sieves for gas separation processes, Gas Sep. Purif. 7 (4) (1993) 247–251.
[20] A.I. Shirley, N.O. Lemcoff, Air separation by carbon molecular sieves, Adsorption 8 (2) (2002) 147–155.
[21] Y. Park, D.-K. Moon, D. Park, M. Mofarahi, C.-H. Lee, Adsorption equilibria and kinetics of CO_2, CO, and N_2 on carbon molecular sieve, Sep. Purif. Technol. 212 (2019) 952–964.
[22] L.A.M. Rocha, K.A. Andreassen, C.A. Grande, Separation of CO_2/CH_4 using carbon molecular sieve (CMS) at low and high pressure, Chem. Eng. Sci. 164 (2017) 148–157.
[23] Y. Yamane, H. Tanaka, M.T. Miyahara, In silico synthesis of carbon molecular sieves for high-performance air separation, Carbon 141 (2019) 626–634.
[24] D.M. Ruthven, N.S. Raghavan, M.M. Hassan, Adsorption and diffusion of nitrogen and oxygen in a carbon molecular sieve, Chem. Eng. Sci. 41 (5) (1986) 1325–1332.
[25] Y. Yamane, M.T. Miyahara, H. Tanaka, High–performance carbon molecular sieves for the separation of propylene and propane, ACS Appl. Mater. Interfaces 14 (15) (2022) 17878–17888.
[26] F. Vallejos-Burgos, F.X. Coudert, K. Kaneko, Air separation with graphene mediated by nanowindow-rim concerted motion, Nat. Commun. 9 (1) (2018) 1812.
[27] A.D. Jannakoudakis, P.D. Jannakoudakis, E. Theodoridou, J.O. Besenhard, Electrochemical oxidation of carbon fibres in aqueous solutions and analysis of the surface oxides, J. Appl. Electrochem. 20 (4) (1990) 619–624.
[28] J.L. Figueiredo, M.F.R. Pereira, M.M.A. Freitas, J.J.M. Órfão, Modification of the surface chemistry of activated carbons, Carbon 37 (9) (1999) 1379–1389.
[29] Z.R. Yue, W. Jiang, L. Wang, S.D. Gardner, C.U. Pittman, Surface characterization of electrochemically oxidized carbon fibers, Carbon 37 (11) (1999) 1785–1796.
[30] R. Berenguer, J.P. Marco-Lozar, C. Quijada, D. Cazorla-Amorós, E. Morallón, Effect of electrochemical treatments on the surface chemistry of activated carbon, Carbon 47 (4) (2009) 1018–1027.
[31] H.-S. Choo, T. Kinumoto, M. Nose, K. Miyazaki, T. Abe, Z. Ogumi, Electrochemical oxidation of highly oriented pyrolytic graphite during potential cycling in sulfuric acid solution, J. Power Sources 185 (2) (2008) 740–746.
[32] M. Nose, T. Kinumoto, H.S. Choo, K. Miyazaki, T. Abe, Z. Ogumi, Electrochemical oxidation of highly oriented pyrolytic graphite in sulphuric acid solution under potential pulse condition, Fuel Cells 9 (3) (2009) 284–290.
[33] V. Presser, C.R. Dennison, J. Campos, K.W. Knehr, E.C. Kumbur, Y. Gogotsi, The electrochemical flow capacitor: a new concept for rapid energy storage and recovery, Adv. Energy Mater. 2 (7) (2012) 895–902.
[34] K.B. Hatzell, E. Iwama, A. Ferris, B. Daffos, K. Urita, T. Tzedakis, F. Chauvet, P.-L. Taberna, Y. Gogotsi, P. Simon, Capacitive deionization concept based on suspension electrodes without ion exchange membranes, Electrochem. Commun. 43 (0) (2014) 18–21.
[35] H. Kaneko, Adaptive design of experiments based on Gaussian mixture regression, Chemom. Intell. Lab Stst. 208 (2021) 104226.
[36] F. Banhart, Irradiation effects in carbon nanostructures, Rep. Prog. Phys. 62 (8) (1999) 1181–1221.
[37] K. Urita, Y. Sato, K. Suenaga, S. Iijima, HR-TEM study of atomic defects in carbon nanostructures, AIP Conf. Proc. 786 (1) (2005) 109–113.
[38] D.A. Shirley, High-resolution X-ray photoemission spectrum of the valence bands of gold, Phys. Rev. B 5 (12) (1972) 4709–4714.
[39] S. Sircar, J.R. Hufton, Why does the linear driving force model for adsorption kinetics work? Adsorption 6 (2) (2000) 137–147.
[40] K. Urita, Y. Sato, K. Suenaga, A. Gloter, A. Hashimoto, M. Ishida, T. Shimada, H. Shinohara, S. Iijima, Defect-induced atomic migration in carbon nanopeapod: tracking the single-atom dynamic behavior, Nano Lett. 4 (12) (2004) 2451–2454.
[41] E. Olsson, J. Cottom, Q. Cai, Defects in hard carbon: where are they located and how does the location affect alkaline metal storage? Small 17 (18) (2021) 2007652.
[42] S. Utsumi, H. Honda, Y. Hattori, H. Kanoh, K. Takahashi, H. Sakai, M. Abe, M. Yudasaka, S. Iijima, K. Kaneko, Direct evidence on C-C single bonding in single-wall carbon nanohorn aggregates, J. Phys. Chem. C 111 (2007) 5572–5575.
[43] C.-M. Yoon, D. Long, S.-M. Jang, W. Qiao, L. Ling, J. Miyawaki, C.-K. Rhee, I. Mochida, S.-H. Yoon, Electrochemical surface oxidation of carbon nanofibers, Carbon 49 (1) (2011) 96–105.